



ELSEVIER

Ultramicroscopy 75 (1998) 161–169

---

---

ultramicroscopy

---

---

# Determination of elastic properties of single aerogel powder particles with the AFM

Robert W. Stark<sup>a</sup>, Tanja Drobek<sup>a</sup>, Marcus Weth<sup>b</sup>, Jochen Fricke<sup>b</sup>, Wolfgang M. Heckl<sup>a,\*</sup>

<sup>a</sup>*Institut für Kristallographie und Angewandte Mineralogie, Universität München, Theresienstr. 41, 80333 München, Germany*

<sup>b</sup>*Bayerisches Zentrum für angewandte Energieforschung e.V. (ZAE Bayern), Am Hubland, 97074 Würzburg, Germany*

Received 26 March 1998; received in revised form 15 August 1998

---

## Abstract

Atomic force microscopy (AFM) allows direct measurement of local elastic sample properties by force spectroscopy. The AFM tip indents into a soft sample and the resulting relation between loading force and indentation is used to determine the elastic properties of the sample. In order to calculate the indentation an analytical expression for the sensor response vs.  $z$ -piezo displacement based on the Hertz model of mechanical contact is derived. This model is fitted to data obtained on a silica aerogel sample using a least-squares method. The aerogel powder particles were analysed individually for their surface structure and elastic behaviour. Prior to the indentation experiments, the aerogel surface was characterised by AFM in the tapping mode. The results were validated by the comparison of data obtained by using two types of cantilevers of very different stiffnesses (spring constant  $k = 0.2$  and  $54$  N/m) and by assessing the reversibility of the indentation process. Tip indentations smaller than  $200$  nm were usually reversible, whereas indentations of  $2000$  nm caused irreversibilities. © 1998 Elsevier Science B.V. All rights reserved.

*PACS:* 61.16.Ch; 62.20.Dc; 61.43.Gt; 81.05.Rm

*Keywords:* Atomic force microscope; Aerogel; Elastic modulus

---

## 1. Introduction

The atomic force microscope (AFM) [1,2] has proven to be a versatile instrument for imaging a wide range of samples with widely different elastic

properties. In AFM measurements like topographic imaging or friction force microscopy the elastic deformations of the sample play an important role [3–6]. In some special cases, a deformation of the tip must be considered, too [7]. However, the indentation of the AFM probe into a sample surface also offers a direct approach to determine elastic sample properties by measuring the sensor response to the  $z$ -piezo displacement [8–10].

---

\* Corresponding author. Tel./fax: + 49 89 23944331; e-mail: w.heckl@lrz.uni-muenchen; <http://www.kri.physik.uni-muenchen.de/crystal/stm/index.htm>.

Silica aerogels are highly porous and transparent or translucent solids, which consist of silicon dioxide. They are produced in a catalytic sol-gel process followed by a suitable drying process generating spongelike open-pore aerogel monoliths or granules [11,12]. This structure consists of “pearl strings” with a diameter of about 5 nm around pores with about 50 nm in diameter (Fig. 1). This structure leads to the special physical properties of aerogels. They have very high porosities (up to 99%) and low densities (as low as  $3 \text{ kg/m}^3$ ) which give rise to low thermal conductivities ( $\lambda \approx 15 \times 10^{-3} \text{ W/mK}$ ), a low refractive index ( $n \ll 1$ ) and a high inner surface (up to  $600 \text{ m}^2/\text{g}$ ). Monolithic aerogels have their applications in high-energy physics as Cherenkov detectors [13] and, because of their high inner surface as catalytic substrate [14], in gas filters [15] or as containment for fusion fuels [11]. For the production of the aerogel powder, the granules are ground. These powders are mainly used as thermal insulations [16,17], with which very low thermal conductivities can be reached in vacuum ( $2 \times 10^{-3} \text{ W/mK}$ ). Another new application for these powders is the use

as a free flowing agent in pharmaceutical engineering. One important property for tailoring aerogels with respect to the desired application is the control of its surface characteristics and elastic properties.

Surface characterisation of silica aerogels with scanning electron microscopy is difficult to achieve, mainly due to charging in the electron beam and destruction of the aerogel surface by the coating process [18]. However, it was possible to obtain images of aerogel surfaces by high-resolution transmission electron microscopy in conjunction with a vertically Pt-C replicated aerogel surface [19]. In contrast to these experimental techniques the AFM allows direct investigation of the untreated specimen surface. Earlier, Borne et al. [20] analysed aerogel particle sizes by comparison of Fourier transformed topographic AFM images to small angle X-ray scattering data. The elastic bulk modulus of silica aerogels has been investigated by measuring sound velocities [21] and mercury porosimetry [22]. In the latter, linear elastic behaviour was found with small strains. For larger strains the network then showed yield followed by densification and plastic hardening.

In the present communication we demonstrate the capability of the AFM for the investigation of material properties like surface topography and elastic modulus of single aerogel powder particles. We address the local elastic properties and possible differences in the elastic behaviour between the bulk and the surface of ground particles. Extending a technique used for very soft biological samples, where the elastic properties have been estimated by the evaluation of selected data points of the sensor response [8,23], we introduce a complete method. All recorded data points of the force curves are analysed and allow a quantitative assessment of the elastic modulus by AFM.

## 2. Materials and methods

### 2.1. Aerogel particles

A commercially available aerogel powder (Basogel, BASF, medium particle size of  $110 \mu\text{m}$ ) was characterised. The heap density is  $110 \text{ kg/m}^3$ ,

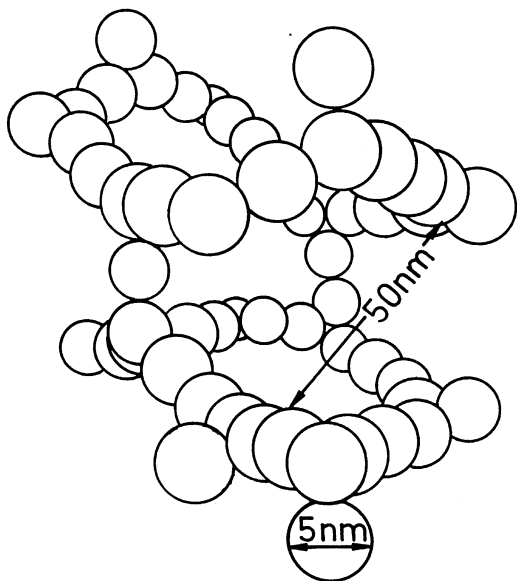


Fig. 1. Schematic diagram of the aerogel structure. About 5 nm sized particles build an open-pore network with about 50 nm sized pores.

which results in a heap porosity of 95%. The aerogel grain density is between 150 and 200 kg/m<sup>3</sup>. The aerogel particles were fixed on a microscope slide on a thin layer of nearly dry enamel. For the Poisson's ratio of the aerogel, a standard value of  $\nu = 0.2$  is assumed [24].

## 2.2. Instrumentation

AFM data were obtained by a commercial instrument (Topometrix Explorer) with 130  $\mu\text{m}$  lateral scan range and a 10  $\mu\text{m}$  z-scanner. The AFM was mounted on top of an inverted microscope (Zeiss Axiovert 135) which allows accurate positioning of the probe on the particles.

The elasticity measurements were done with an Si cantilever (nanosensors, pyramidal tip shape, cone half angle  $\alpha = 18^\circ$ , tip curvature radius  $r \leq 10$  nm, resonant frequency nominal: 17 kHz, measured: 11.80 kHz,  $Q = 26$ ). The spring constant ( $k = 0.19$  N/m) was determined using the method of thermal fluctuations [25,26].

For control experiments a stiff Si cantilever was employed (nanosensors, spring constant  $k = 54$  N/m, pyramidal tip shape, tip height 10  $\mu\text{m}$ , cone half angle  $\alpha = 18^\circ$ , tip curvature radius  $r \leq 10$  nm, resonant frequency nominal: 350 kHz, measured: 361 kHz). This cantilever was characterised individually by the manufacturer. The relative error of the spring constant is estimated by the manufacturer to be 20%. All experiments were performed in ambient conditions with a relative humidity of 40%. Imaging was done in high amplitude resonant mode (tapping mode, 1 Hz scan rate). The setpoint was 60% of the free oscillation far away from the surface.

## 2.3. Force curve measurements

A series of force curves was obtained at the same position on the particles. To avoid structural damage of the aerogel sample at the point of interest, the tip was first approached carefully to the sample surface. Then, the tip was retracted by adjusting the setpoint to the lowest possible value. Subsequently, the force curve measurements were performed at a distance of a few microns (approx. 20  $\mu\text{m}$ ) away

from the original contact point. This procedure was necessary to assess changes in the shape of the force curves due to sample deterioration induced by the tip. For force curve acquisition the upper force limit was set to 50 nN. In order to minimize piezo hysteresis effects the z-approach speed was 1  $\mu\text{m/s}$ . Before and after the measurements on each particle, the sensor response was calibrated on the glass substrate.

A set of control experiments was performed using a stiff cantilever. The first approach was done in the tapping mode, the following experimental procedure was the same as before.

## 3. Data analysis

The indentation of an AFM tip fixed to a cantilever (spring constant  $k$ ) into a soft sample (Young's modulus  $E$ , Poisson's ratio  $\nu$ , i.e. the ratio of longitudinal extension to transverse contraction) can be modelled using Hertzian contact mechanics [27]. This theory provides a very simple but direct approach to the sample elasticity.

For an infinitely hard body indenting (indentation  $d$ ) into an elastic half space with a normal force  $F$  this theory leads to:

$$F = \zeta d^m \frac{E}{1 - \nu^2}, \quad (1)$$

where  $\zeta$  is a constant dependent on the tip geometry. The exponent  $m$  characterises the indentation behaviour. For the indentation of a sphere the exponent is  $m = \frac{3}{2}$  ( $d \ll$  sphere radius). A cone with a half angle  $\alpha$  leads to  $m = 2$  and  $x = \frac{1}{2}\pi \tan \alpha$ .

The indentation cannot be measured directly by AFM, because the data are usually obtained as a photodiode signal (i.e. the cantilever deflection) vs. z-piezo displacement curve. This curve is referred to as the force curve. Basically, a force curve can be divided into two different regions. With the tip off the surface the cantilever deflection is constant. However, when the tip is in contact with the sample, the force curve is sloped. The slope depends on the stiffness of the sample. For an infinitely hard sample and tip, the deflection  $d(z)$  of the cantilever, i.e. the force curve, can be described by the

expression,

$$\delta(z) = \begin{cases} -(z - z_0), & z < z_0, \\ 0, & z \geq z_0, \end{cases} \quad (2)$$

where  $z_0$  is the  $z$  piezo position when the tip hits the sample (contact point).

Force curves on soft samples can be calculated directly from the Hertz model in Eq. (1). Assuming a cone as a model for the AFM tip, the cantilever deflection vs. indentation relation is

$$d(z) = \left( k\delta(z) \frac{2}{\pi \tan \alpha} \frac{1 - \nu^2}{E} \right)^{1/2}, \quad (3)$$

where  $F(z) = k\delta(z)$  is the loading force. Considering the indentation  $d(z)$ , the cantilever deflection in Eq. (2) for soft samples becomes

$$\delta(z) = \begin{cases} -(z - z_0) - d(z), & z < z_0, \\ 0, & z \geq z_0. \end{cases} \quad (4)$$

Inserting Eq. (3) into Eq. (4) and solving the quadratic equation, the expression for the force curve  $d(z)$  on an elastic sample is

$$\delta(z) = \begin{cases} \frac{a}{K} - (z - z_0) \mp \left[ \frac{a^2}{K^2} - 2\frac{a}{K}(z - z_0) \right]^{1/2}, & z < z_0, \\ 0, & z \geq z_0, \end{cases} \quad (5)$$

with

$$a = \frac{k}{\pi \tan \alpha} \quad \text{and} \quad K = \frac{E}{1 - \nu^2}. \quad (6)$$

$K$  is referred to as the elastic constant. In Eq. (5) the solution with the negative sign is the physically relevant root. For an infinitely hard substrate, the slope of the force curve is equal to  $-1$  in contact regime (see also Eq. (2)).

In order to calculate the indentation from the experimental force curve data a precise knowledge of the contact point  $z_0$  is necessary. Often,  $z_0$  cannot be read directly from the force curve data, because additional forces like electrostatic interac-

tion and meniscus forces, which are neglected in the Hertzian contact mechanics model, are dominant in the region of a few nanometres around the contact point. This region can be referred to as “transition region” [9]. The contact point  $z_0$  together with  $E$  and an offset of the force curve from the abscissa is estimated from the experimental data by nonlinear regression (Levenberg–Marquardt algorithm [28]). The main advantage of this approach is that the point of mechanical contact is calculated from data where the elastic deformation of the sample yields the dominant forces. This allows accurate calculation of the indentation into the sample in the picture of Hertzian contact mechanics.

## 4. Results and discussion

### 4.1. Imaging

Atomic force microscopy of the fragile aerogel revealed a rough structure (Fig. 2). For the indentation experiment using the stiff cantilever, the sample was first scanned in the high amplitude resonant (tapping) mode. To inspect the region of interest a series of images was recorded decreasing the scan range stepwise. Fig. 2b is the first zoom into the centre of Fig. 2a. Further reduction of the scan-range did not enhance resolution (data not shown). To reveal more contrast, the corresponding error signal is given in Fig. 2c and Fig. 2d). Several pores on the surface can be identified (Fig. 2b) as indicated by the arrows. Obviously, the investigation of pores is limited by the tip geometry and its aspect ratio. Particles smaller than 50 nm in diameter could not be resolved. This limitation is caused by the flexibility of the aerogel sample and by tip–sample convolution. After imaging, force curve measurements were performed.

In a second set of experiments the repeatability of the scanning process itself was examined. When scanning the same region of interest repeatedly, the tip was contaminated by aerogel debris on the sample surface and the resolution decreased after about ten scans. Imaging in contact mode was impossible.

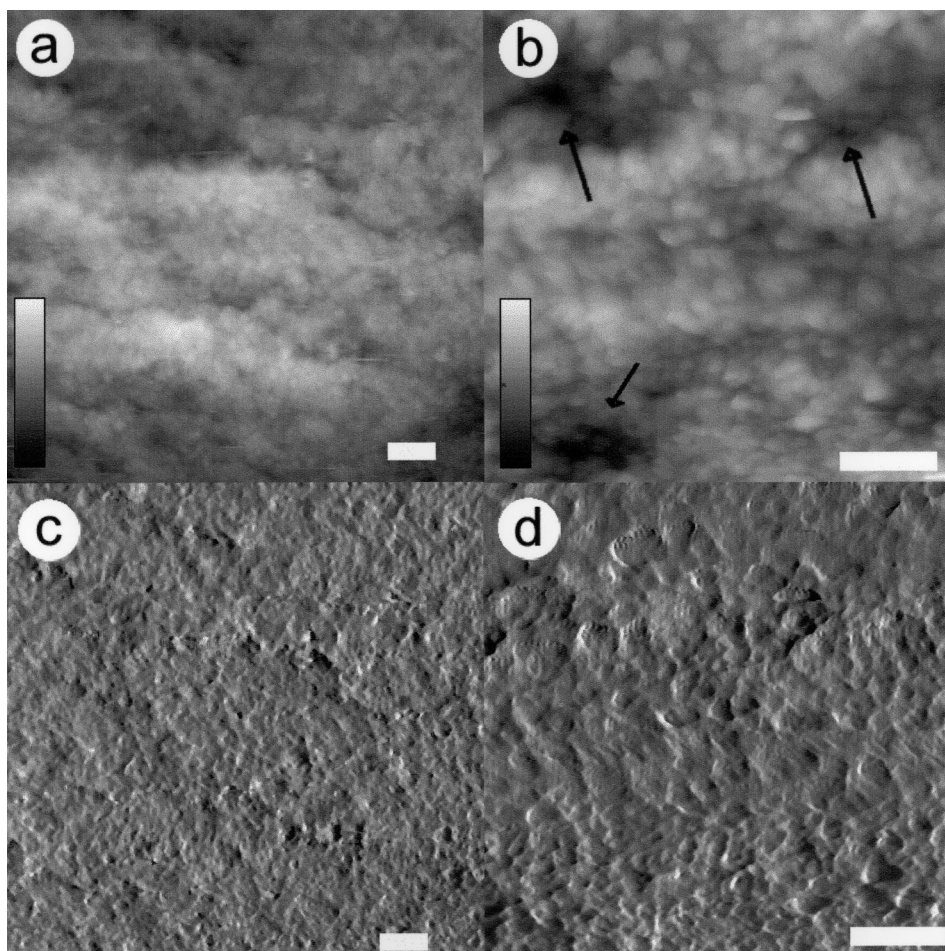


Fig. 2. AFM micrographs obtained in the tapping mode on an untreated silica aerogel surface in ambient conditions. The upper images show surface topography, below is the corresponding error signal. (a) z-scale bar is 0...1400 nm, scale bar is 1  $\mu\text{m}$ . (b) z-scale 0...800 nm, scale bar 1  $\mu\text{m}$ . The arrows point to pores. The roughness of this area is  $R_{\text{rms}} = 158 \text{ nm}$  (c,d) scale bar: 1  $\mu\text{m}$ .

## 4.2. Indentation experiments

### 4.2.1. Experiments with soft cantilevers

Probing a rough sample surface with an AFM tip, different types of probe-sample contact can be expected. (i) The tip indents into a flat surface (Fig. 3) and the process can be described by Hertzian contact mechanics (ii) If the probe interacts with protrusions on the surface, the sample stiffness can be modelled by a Hook spring with a force constant  $k_s$ , leading to a linear sensor response signal (Fig. 4). Some force curves with intermediate behaviour were also found (data not shown).

In Fig. 3a the first force curve in the approach direction is displayed. This force curve was selected for presentation because it shows both, structural breakdowns and elastic response. (For a typical elastic response curve see Fig. 5.) A transition region with several structural breakdowns was observed for z-positions from 240 nm to 100 nm. Outside of this transition region the experimental data can be described by the model Eq. (5). At the bottom of Fig. 3a, the residue between data and the model is plotted. For curve fitting, the data in the greyed transition region were omitted. From this fit the contact point  $z_0$  on the flat surface set was

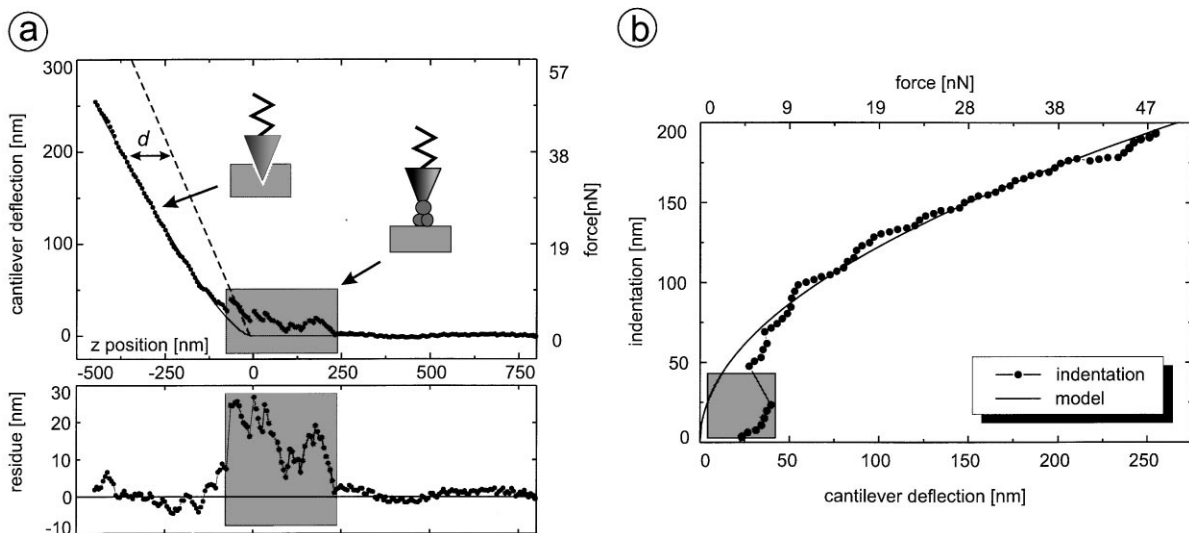


Fig. 3. Indentation experiment on the aerogel surface showing the elastic response (soft cantilever  $k = 0.19$  N/m). (a) Fit of the experimental force curve data in the approach direction to the model Eq. (5). The residue is plotted below. A force curve on an infinitely hard substrate is shown as a dashed line. The indentation  $d$  of the tip into the sample is the difference between the force curve on the elastic sample and a hard sample as indicated by the horizontal arrow. The corresponding fit parameters are: elastic constant  $E/(1 - \nu^2) = 5.36$  MPa and  $z_0 = 0$  nm. Between 240 nm and  $-100$  nm  $z$ -position there is a transition region (grey), where the structure collapses several times. At lower  $z$ -positions the force curve exhibits elastic behaviour. (b) Resulting indentation vs. force plot with good agreement between data and model.

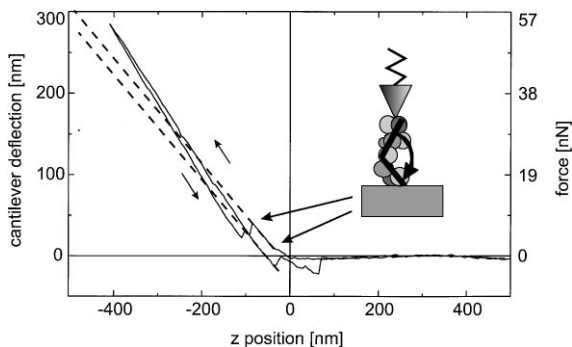


Fig. 4. Linear response in an indentation experiment on the aerogel surface (soft cantilever,  $k = 0.19$  N/m). Approach and retraction directions are indicated by the small arrows. The curve exhibits two instability points (arrows). Between these instabilities the force curve is linear. After each structural change the spring constant increases (see extrapolated linear sections). Correspondingly, there are rupture events in the retraction direction.

calculated. This allowed subsequent calculation of the indentation of the tip into the sample (Fig. 3b). Outside the transition region the model fits the data well. The least-squares estimate for the

Young's modulus is  $E = 5.15$  MPa with a statistical uncertainty of  $\pm 0.12$  MPa. The real uncertainty maybe much larger, mainly due to the error in the spring constant of the cantilever. The advantage of the least-squares method is now clearly visible. The parameter  $z_0$ , which cannot be obtained directly from the force curve, because the structural breakdown and the change in elastic response hide the contact point, could now be determined. The behaviour in the transition region can be interpreted by a surface protrusion which is first hit by the tip. With increasing loading force this protrusion broke down irreversibly in several steps until the probe was in solid mechanical contact with the bulk.

In a series of five identical experiments on different particles an average elastic modulus of  $E = 5.4$  MPa was measured. The results varied from  $E = 2.7$  MPa to  $E = 8.6$  MPa.

A force curve exhibiting a linear response is shown in Fig. 4. As before, a force curve indicating structural changes has been selected, though force curves without peculiarities were found, too. In the

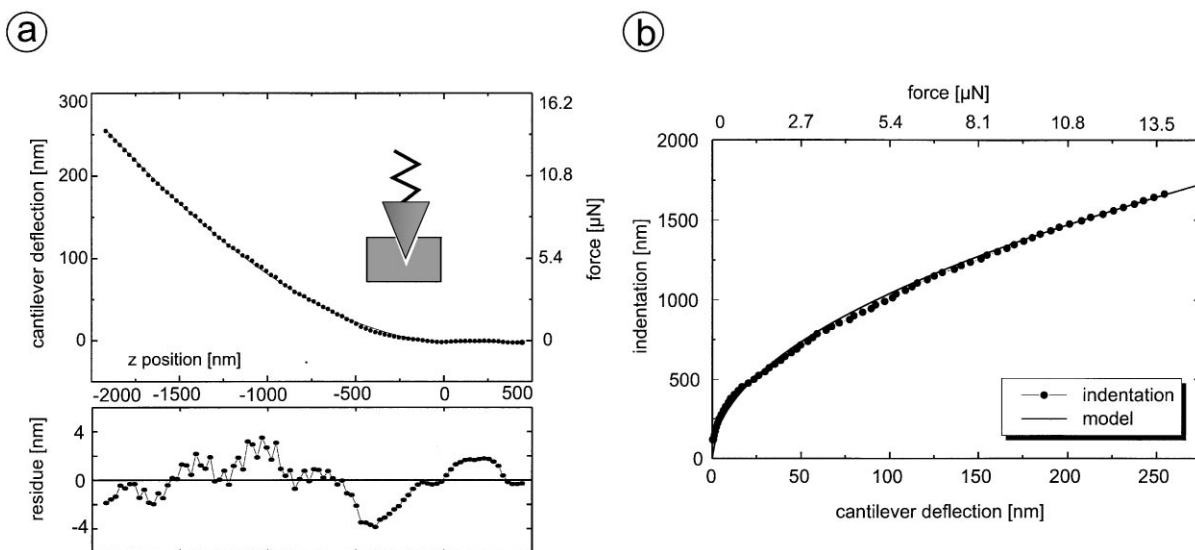


Fig. 5. Purely elastic response in an indentation experiment on the aerogel surface (stiff cantilever,  $k = 54$  Nm). Note that here forces are given in  $\mu\text{N}$ . (a) Fit of the experimental data in the approach direction to the model Eq. (5). Fit parameters: elastic constant  $E/(1 - \nu^2) = 8.9$  MPa and  $z_0 = -29$  nm. Below, the residue between data and the model is plotted. (b) The resulting indentation vs. force plot shows excellent agreement between data and the model.

approach direction two instabilities ( $F = 2$  nN,  $F = 8$  nN) were observed as indicated. Beyond each instability point the slope of the force curve, i.e. the force constant  $k_s$  of the sample, is increased. During retraction, rupture events coincide with the instabilities in the approach direction. The slopes of the retraction curve in this area are similar to the corresponding slopes in the approach direction. This indicates that the process of structural changes induced by the tip is reversible. Thus, the instabilities are explained by a configuration in the protrusion that acts as a joint. At a certain loading force the joint snaps over. Due to this configurational change the spring constant of the system is changed.

These observations together with the fact that the tip usually is contaminated during scanning show that the surface of an aerogel particle is covered with irregular and instable structures which also determine the adhesion behaviour between different particles in powders used for industrial applications.

#### 4.2.2. Experiments with stiff cantilevers

A series of control experiments was performed using a stiff cantilever. The applied loading forces

were increased by two orders of magnitude as compared to the experiments with soft cantilevers. The main goal of these measurements was to probe sample elasticity deeper within the bulk of the particles.

All indentation experiments can be described by the mechanical contact theory (Eq. (5)). The loading forces were much higher than before, leading to a decreased force sensitivity. Fig. 5a shows a typical force curve in the approach direction. The calculated indentation is in excellent agreement with the experimental data (Fig. 5b). Indentations up to  $2 \mu\text{m}$  were performed. Although this is by a factor 10 higher than in the experiments above, the model fits the data well. The least-squares estimate for the elastic modulus is  $E = 8.1 \pm 0.7$  MPa. The average out of five experiments was  $E = 6.9$  MPa with numerical values from  $E = 5.8$  MPa to  $E = 9.1$  MPa. From the fact that this value is similar to the one measured with only 200 nm indentation we concluded that the aerogel surface, even after the grinding process, has similar elastic properties as the bulk.

In Ref. [21] sound velocities in different aerogels were measured. For silica aerogels in air with

$\rho = 150 \text{ kg m}^{-3}$  ( $\rho = 200 \text{ kg}^{-3}$ ), a sound velocity of about  $c = 180 \text{ m s}^{-1}$  ( $c = 300 \text{ m s}^{-1}$ ) was found. Thus, the Young's modulus was  $E = 4.9 \text{ MPa}$  and  $E = 18 \text{ MPa}$ , respectively. Our values confirm these results.

Deep indentations also can cause structural collapses. Fig. 6 shows a series of consecutive indentation experiments. A massive break down was observed in Fig. 6 d) where the structure collapsed and the force curve was shifted about  $1 \mu\text{m}$  to the left. In the retraction direction no single rupture events can be found. This was expected because the forces for ruptures were found to be in the order of  $20 \text{ nN}$ . The forces in this experiment are two orders of magnitude higher, therefore single events cannot be resolved. These experiments indicate that it is necessary to validate indentation experiments carefully in order to avoid plastic deformations where elastic ones are desirable. Here, the indentation into the aerogel sample induced irreversible structural changes. Nevertheless, forces in the order of micronewtons were needed to induce irreversible collapses.

## 5. Conclusions

The determination of local elastic sample properties by measuring the sensor response of an AFM tip indenting into a soft sample using a mechanical contact model together with a least-squares method has been introduced. This method was applied to single silica aerogel particles. After imaging the aerogel surface by AFM the Young's modulus  $E$  has been determined to be in the order of  $E = 6 \text{ MPa}$ . This value confirms earlier measurements of sound velocities in monolithic aerogels. It was found that the value for  $E$  varies somewhat with the position on the aerogel. The reversibility of the indentation experiments was investigated. For loading forces in the order of  $10 \text{ nN}$ , reversible processes were found whereas at higher loading forces in the order of  $1 \mu\text{N}$ , irreversibilities can occur. The main advantage of the introduced method of data analysis is that it uses a large number of data points (typically 200–500) and consequently allows the exact determination of the contact point  $z_0$ . Thus, the local Young's modulus

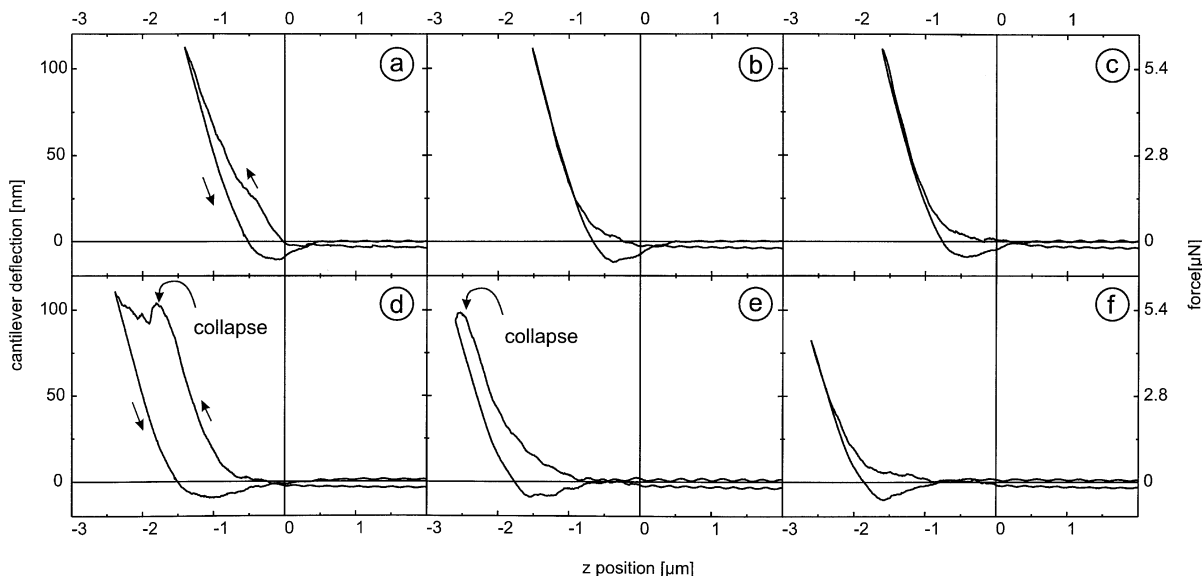


Fig. 6. Series of indentation experiments (stiff cantilever). The first six consecutive indentations of a series of fifty are shown. (a) Force curve exhibiting slight structural changes. (b,c) Subsequent force curves showing elastic behaviour. (d) A structural collapse in the order of about  $1 \mu\text{m}$  in depth. (e) The aerogel structure collapses again. (f) Elastic behaviour that cannot be explained entirely by the model in Eq. (5). The force curve in (f) is shifted about  $1.5 \mu\text{m}$  to the left as compared to (a). Nevertheless, the elastic response is still similar to the force curve in (a).

can be measured for samples where the transition region from noncontact to mechanical contact shows a complex behaviour.

### Acknowledgements

We thank F. Bernhard for the fruitful discussions. This work was supported by the Bayerische Forschungsstiftung (RWS) and DFG grant He-1617/7-1 (TD).

### References

- [1] G. Binnig, C.F. Quate, C. Gerber, *Phys. Rev. Lett.* 56 (1986) 930.
- [2] G. Binnig, C. Gerber, E. Stoll, T.R. Albrecht, C.F. Quate, *Europhys. Lett.* 3 (1987) 1281.
- [3] G. Overney, W.Q. Zhong, D. Tomanek, *J. Vac. Sci. Technol. B* 9 (1991) 479.
- [4] M. Specht, F. Ohnesorge, W.M. Heckl, *Surf. Sci. Lett.* 257 (1991) L653.
- [5] G. Overney, D. Tomanek, W. Zhong, Z. Sun, H. Miyazaki, S.D. Mahanti, H.J. Güntherodt, *J. Phys.: Condens. Matter* 4 (1992) 4233.
- [6] N.J. Tao, S.M. Lindsay, S. Lee, *Biophys. J.* 63 (1992) 1165.
- [7] M. Heuberger, G. Dietler, L. Schlapbach, *J. Vac. Sci. Technol. B* 14 (1996) 1250.
- [8] M. Radmacher, M. Fritz, P.K. Hansma, *Biophys. J.* 69 (1995) 264.
- [9] M.R. Vanlandingham, S.H. Mcknight, G.R. Palmese, R.F. Eduljee, J.W. Gillespie, R.L. Mcculough, *J. Mater. Sci. Lett.* 16 (1997) 117.
- [10] R.W. Stark, S. Thalhammer, J. Wienberg, W.M. Heckl, *Appl. Phys. A* 66 (1998) S579.
- [11] G.A. Nicolaon, S.J. Teichner, *Bull. Soc. Chim. Fr.* (1968) 1906.
- [12] S.S. Kistler, *Nature* 127 (1931) 741.
- [13] M. Cantin, M. Casse, L. Koch, R. Jouan, P. Mestran, D. Roussel, F. Bonnin, J. Moutel, S.J. Teichner, *Nucl. Instrum. Meth.* 118 (1974) 177.
- [14] G.M. Pajonk, *Appl. Catalysis* 72 (1991) 217.
- [15] D.W. Cooper, *Part. Sci. Technol.* 7 (1989) 371.
- [16] J. Fricke, *Thermal Transport in Porous Superinsulations*, in: J. Fricke (Ed.), *Aerogels*, Springer, Heidelberg, 1986, p. 110.
- [17] E. Hummer, T. Rettelbach, X. Lu, J. Fricke, *Thermochimica Acta* 218 (1993) 269.
- [18] E. Courtens, R. Vacher, *Phil. Mag. B* 65 (1992) 347.
- [19] G.C. Ruben, L.W. Hrubesh, T.M. Tillotson, *J. Non-Cryst. Solids* 186 (1995) 209.
- [20] A. Borne, B. Chevalier, J.L. Chevalier, D. Quenard, E. Elaloui, J. Lambard, *J. Non-Cryst. Solids* 188 (1995) 235.
- [21] J. Groß, J. Fricke, R.W. Pekala, L.W. Hrubesh, *Phys. Rev. B* 45 (1992) 12774.
- [22] G.W. Scherer, D.M. Smith, X.M. Qiu, J.M. Anderson, *J. Non-Cryst. Solids* 186 (1995) 316.
- [23] U.G. Hofmann, C. Rotsch, P.W.J.M. Radmacher, *J. Struct. Biol.* 119 (1997) 84.
- [24] J. Groß, G. Reichenauer, J. Fricke, *J. Phys. D* 21 (1988) 1447.
- [25] J.L. Hutter, J. Bechhoefer, *Rev. Sci. Instr.* 64 (1993) 1868.
- [26] H.J. Butt, M. Jaschke, *Nanotechnology* 6 (1995) 1.
- [27] H. Hertz, *J. Reine Angew. Math.* 92 (1888) 156.
- [28] W.H. Press et al., *Numerical Recipes in C*, Press Syndicate of the University of Cambridge, Cambridge, 1992.